1

Spatially-Consistent Human Body Blockage Modeling: A State Generation Procedure

Margarita Gapeyenko, Andrey Samuylov, Mikhail Gerasimenko, Dmitri Moltchanov, Sarabjot Singh, Mustafa Riza Akdeniz, Ehsan Aryafar, Sergey Andreev, Nageen Himayat, and Yevgeni Koucheryavy

Abstract—Spatial correlation has been recognized by 3GPP as one of the key elements in millimeter-wave (mmWave) channel modeling. Correlated channel behavior is induced by macro objects, such as buildings, as well as by micro objects, including humans around the mmWave receivers. The 3GPP's three-dimensional (3D) spatially consistent channel model designed to capture these phenomena assumes a-priori knowledge of the correlation distance between the receivers. In this paper, we propose a novel spatially-consistent human body blockage state generation procedure, which extends the standardized 3D channel model by 3GPP to capture the correlation between the line-of-sight (LoS) links and the reflected cluster states affected by human body blockage. The proposed model is based on analytical expressions for the conditional link state probability, thus permitting the parametrization of the spatial field of receivers. It also does not require any a-priori information on the correlation distance as the latter is identified explicitly based on the environmental parameters. We compare the results for the proposed model with those obtained with the uncorrelated blockage model and conclude that in many special cases correlation manifests itself in quantitatively different propagation conditions experienced at the nearby receivers.

Index Terms—5G, mmWave, 3GPP 3D channel model, human body blockage, spatial consistency, correlation.

1 Introduction

Millimeter-wave (mmWave) communication is considered to be the core part of the emerging 5G mobile networks, which are capable of supporting the stringent requirements of IMT-2020 [1]. Larger available bandwidths make the extremely high frequency bands an attractive candidate for serving advanced future applications [2]–[5].

Despite a number of benefits delivered by mmWave, there are also several challenges to be solved. For example, due to shorter wavelengths, smaller objects in the channel may produce a considerable impact on the mmWave propagation. According to the recent studies, human body blockage leads to a significant attenuation of the mmWave signal [6]–[8] and should be taken into account in mmWave channel modeling [9], [10].

An example of such models is the 3GPP three-dimensional (3D) stochastic channel model (SCM) proposed in [11] that has further been improved and ratified by 3GPP in Release 15 [9]. It is currently utilized by both academia and industry to capture the mmWave channel properties in system-level simulators (SLS) [12], [13].

If mmWave-based receivers are located next to one another, they often experience similar propagation

M. Gapeyenko, A. Samuylov, M. Gerasimenko, D. Moltchanov, S. Andreev, and Y. Koucheryavy are with Tampere University, Tampere, Finland (e-mail: {firstname.lastname, evgeni.kucheryavy}@tuni.fi).
S. Singh is with Uhana (e-mail: sarabjotsingh.in@gmail.com)
M. R. Akdeniz and N. Himayat are with Intel Corporation, Santa Clara,

CA, USA (e-mail: {mustafa.akdeniz, nageen.himayat}@intel.com)
E. Aryafar is with Portland State University, Portland, OR, USA (e-mail: earyafar@gmail.com)

conditions [14]–[16]. This effect, known as *spatial correlation*, has been recently recognized by 3GPP as an important consideration in the mmWave channel modeling [9]. The correlated state of the channel at the receiver (Rx) may affect implementation and performance of beamsearching and beamtracking mechanisms, resource allocation strategies, as well as multiple-input multiple-output (MIMO) system design [9], [17]–[20].

1.1 Background and Related Studies

3GPP has recently extended its 3D SCM channel model to capture the correlation of large and small scale parameters (LSP and SCP) as well as (non)-line-of-sight (n)LoS states. In [9], [21], three such methods have been proposed. In the first one, named *method of spatially-consistent random variables*, the spatial correlation of channel clusters is accounted for by introducing the so-called spatial consistency to the channel cluster specific random variables taken from the 3GPP 3D SCM model [9].

The second method is known as *geometric stochastic approach*. In this case, the large scale parameters (LSP) are pre-computed for every grid, and each Rx inside it is associated with these LSP. The grid has a rectangular shape with the side length of correlation distance that is provided a-priori. In the third alternative, called *method of geometrical cluster locations* (grid-based GSCM, GGSCM), the cluster, path angles, and delays are defined by the geometrical positions (x, y) of the appropriate scatterers. In all these models, the correlation distance is arbitrarily chosen as an

input parameter, which leads to non-uniqueness of the resulting propagation environment.

With the help of a ray-based simulator, the authors in [22] demonstrated a profound impact of spatial consistency on the path loss modeling. The work in [23] described a spatially consistent path loss model for the street urban scenarios. In [24], the authors presented their simulator wherein the spatially consistent channel model is integrated.

In addition to macro objects affecting the LoS/nLoS state, smaller objects (e.g., humans, vehicles, etc.) induce blockage of the mmWave channel. When modeling highly crowded realistic urban environments, such as squares and stadiums, the use of ray-tracing approaches is often difficult due to the associated computational complexity. Recently, a number of analytical models for blockage phenomena were proposed [25]-[27]. However, these constructions either do not capture the effect of spatial correlation or do not offer a method to optimize the channel model. In [28], the authors measured the channel from different base station (BS) locations and demonstrated how the knowledge of correlation distance may help find another best BS in case of blockage. Further, in [29], the authors argued for the importance of correlated blockage consideration. They proposed a model to establish the probability that a certain target is blocked, while having more than one transceiver communicating with that target.

Recently, there have been multiple attempts within 3GPP to extend the SCM model by capturing the spatial correlation of blockage caused by micro objects, including the human crowd [9]. Particularly, in [9], a human body has been modeled and two blockage models, namely, A and B, were introduced. The model A stochastically generates M 2D blockage regions uniformly distributed around each Rx. The parameter M is a fixed number that may be changed in case the density of blockers varies. The latter model does not account for the height of blockers and assumes a fixed distance between Rx and blocker, which significantly reduces the applicability of this model. In order to account for the spatial correlation between blockers, a certain autocorrelation function is applied to the centers of blockers. The limitation of this model is in the correlation distance, which is a parameter that needs to be specified in advance.

In model *B*, a total of *M* rectangular screens are physically placed on a map. This allows to account for any density, dimensions of blockers, as well as spatial consistency during the simulation time. However, the computational complexity of this method increases significantly with the growing numbers of blockers, thus making it infeasible to apply for modeling densely crowded environments.

1.2 Contributions of This Work

In this paper, we complement the existing 3GPP 3D channel model for the frequencies of 0.5 to 100 GHz [9] by accounting for the spatial correlation caused by micro objects (particularly, humans bodies) in crowded scenarios, e.g., squares, stadiums, etc. Particularly, we propose a novel spatially consistent blockage state generation procedure, which employs our analytical framework for the conditional link state probabilities. Compared to 3GPP blockage models, our approach features the following advantages: (i) correlation distance does not need to be specified in advance, (ii) spatial correlation is captured across all of the blockers, and (iii) computational complexity does not depend on the density of blockers, which makes it possible to model crowded environments.

Our main contributions are therefore as follows:

- We analyze the spatial correlation of human body blockage caused by a dense crowd around the receivers for the mmWave channel by proposing a novel mathematical framework. We derive the conditional channel state probabilities for every link generated within the scenario, such as Transmitter-Rx links or Reflector-Rx links;
- We integrate the proposed analytical model into the SLS software [30], with our new blockage state generation procedure taking into account the actual correlation across micro objects. This blockage generation procedure allows to optimize the channel model by introducing an additional channel state (blocked/non-blocked) for every link, which captures the spatiallyconsistent human body blockage;
- We characterize the absolute received power difference when disregarding the correlation due to micro objects in the mmWave channel by conducting extensive simulations. We thus demonstrate that the spatial correlation is a local effect, which leads to significant received power variations at nearby locations when it is not accounted for.

The rest of this paper is organized as follows. The system model and its assumptions are introduced in Section 2. Our mathematical framework is developed in Section 3. The spatially-consistent blockage state generation procedure for mmWave propagation modeling is outlined in Section 4. The key numerical results are reported in Section 5. Conclusions are drawn in the last section.

2 System Model and Assumptions

2.1 Propagation Environment

The considered scenario is illustrated in Fig. 1. The transmitter (Tx) is assumed to be located at the origin and has the height of h_T . The human body blockers (referred to as blockers further on) are uniformly

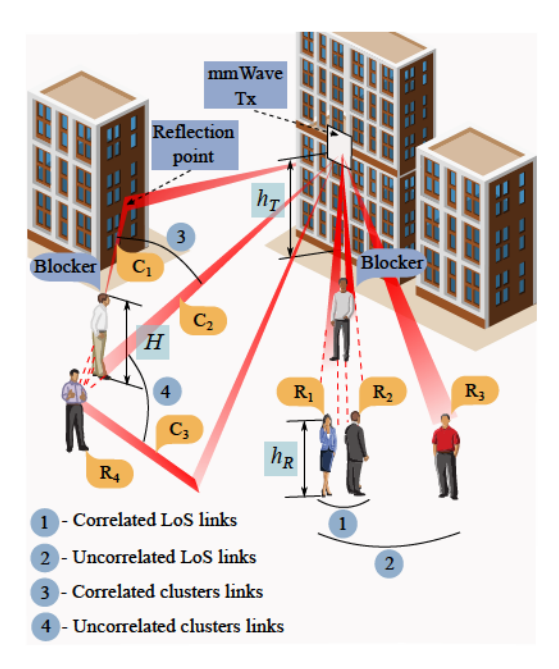


Fig. 1. The considered scenario of interest.

distributed in the area and modeled as cylinders [31] with the random height of H as well as the constant base diameter of d_m . The blocker heights are assumed to be approximated by a Normal distribution $H \sim N(\mu_H, \sigma_H)$ [32]. The centers of the cylinder bases follow a 2D Poisson point process (PPP) with the density of λ_B . A total of K Rx are uniformly distributed in the area S with the coordinates $x_{R,k}, y_{R,k}, k = 1, \ldots, K$. The size of Rx is assumed to be infinitesimally small. The rest of the parameters are summarized in Table 1.

As one may observe in Fig. 1, there are multiple *clusters* arriving at Rx.

TABLE 1 Summary of notation and parameters

Notation	Description
h_T , h_R	Height of Tx, Rx
$x_{R,k}, y_{R,k}$	x-, y- coordinates of Rx k , $k = 1,, K$
x_T, y_T	x-, y- coordinates of Tx
$x_{C,kn}, y_{C,kn}, z_{C,kn}$	x-, y-, z- coordinates of reflecting point for cluster n of Rx k
$\phi_{D,kn}, \phi_{A,kn}$	Angles of departure and arrival of cluster n
$\theta_{D,kn}$, $\theta_{A,kn}$	Zenith angles of departure and arrival of clus-
	ter n
$ au_{kn}$	Delay of cluster n
H , d_m	Height and diameter of a blocker, $H \sim$
	$N(\mu_H, \sigma_H)$
$F_H(x)$	CDF of the blocker height
λ_B	Density of blockers per unit area
h_C , h_1 , h_2	Heights of points P , O , and M
r_0	Two-dimensional distance from O to P
d	Two-dimensional distance from O to M
α	Angle $\angle POM$
p_{00} , p_{01}	Conditional probabilities to reside in non-
	blocked/blocked states at point M (0 and 1)
	given that there was non-blocked state at O
p_{10}, p_{11}	Conditional probabilities to reside in non-
	blocked/blocked states at point M (0 and 1)
	given that there was blocked state at O

Definition 1. A cluster is a set of rays that travel from Tx to Rx with a small variation in their angles of arrival and departure caused by diffuse reflections on the same surface.

The correlation between the current channel states of the links is a consequence of the separation angle of clusters. Particularly, two Rx, R_1 and R_2 , in Fig. 1 are located nearby, which leads to the correlation between their LoS links. In contrast, R_1 and R_3 are well-separated, which implies that the presence of blockage at R_1 does not affect LoS link at R_3 . The situation is similar with the clusters. Two clusters, C_1 and C_2 , arriving at Rx R_4 are correlated with each other as they are not well-separated in space, and a single blocker occludes their paths. At the same time, clusters C_2 and C_3 are independent. A spatially-consistent model for mmWave channel needs to take the effects of spatially-consistent human body blockage into account.

2.2 3GPP 3D Channel Model

It is important to note that the proposed blockage state generation procedure is compatible with any channel model. Below, we briefly review the 3GPP models with and without spatial correlation as they are widely acceptable. 3GPP 3D channel model for bands higher than 6 GHz was introduced in [9]. The proposed considerations are based on a similar logic as those in the LTE specifications [33], with modifications specific to mmWave frequencies. The model thus allows to generate a set of correlated (with each other) parameters (angle-of-departure (AoD), angle-of-arrival (AoA), zenith-of-departure (ZoD), zenith-of-arrival (ZoA), powers, delays, etc.) for each cluster based on the measurements conducted in a specific radio environment.

In Section 7.6.3 of [9], a spatially-consistent extension to the 3GPP 3D channel model is proposed. The modeling procedure comprises two parts: 1) generation of spatially-consistent large scale and small scale parameters for a static Rx drop; and 2) correlated Rx mobility modeling. In step one, a regular horizontal grid is generated, whose inter-site distance equals the correlation distance specified in advance. The standard mmWave model is used to specify the propagation conditions for each node of the grid. The propagation parameters of Rx are then interpolated based on the nearest nodes, see [34] for details. When Rx mobility is added, the delay, departure/arrival angles, and cluster powers are updated according to user direction and speed.

2.3 3GPP Cluster Localization Process

According to the 3GPP 3D channel model, there are N clusters arriving at every Rx in the scenario, where N is a scenario-specific parameter [9]. The model _provides the AoA, AoD, ZoD, ZoA, delay, etc. for

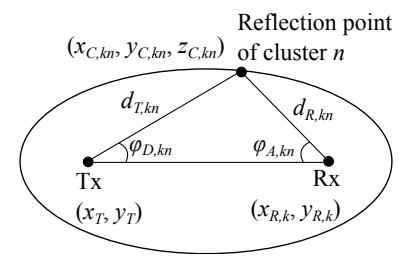


Fig. 2. Illustration of location of a cluster.

each cluster, which become the input parameters for our analytical framework outlined in Section 3. To introduce our spatially-consistent blockage state generation procedure described in Section 4 based on the novel analytical framework introduced in Section 3, it is also required to obtain the coordinates of the cluster's reflection points for Rx k, $(x_{C,kn}, y_{C,kn}, z_{C,kn})$. In order to do that, we follow [21] by assuming that Tx and Rx are located at the foci of an ellipse, and that the reflection point of a single bounce is located at the arc of this ellipse as shown in Fig. 2. With this method, we can extract the x-, y-, and z-coordinates of the reflecting point of cluster n for Rx k, which are required to parametrize our analytical framework, as follows:

- as the random generation of AoA and AoD according to 3GPP [9] does not guarantee that the arrival and departure clusters will intersect in 3D space, we randomly choose Tx-side or Rx-side;
- compute the coordinates $(x_{C,kn}, y_{C,kn})$ as:
 - choosing Tx-side, we have:

$$x_{C,kn} = x_T + d_{T,kn} \cos \phi_{D,n},$$

 $y_{C,kn} = y_T + d_{T,kn} \sin \phi_{D,n}.$ (1)

- alternatively, choosing Rx-side we have:

$$x_{C,kn} = x_{R,k} + d_{R,kn}\cos\phi_{A,kn},$$

 $y_{C,kn} = y_{R,k} + d_{R,kn}\sin\phi_{A,kn},$ (2)

where $d_{T,kn}$ and $d_{R,kn}$ are the distances between the reflecting point of cluster n and Tx or Rx k, respectively, x_T , y_T , $x_{R,k}$, and $y_{R,k}$ are the coordinates of Tx and Rx k, $\phi_{D,kn}$ and $\phi_{A,kn}$ are the angles of departure and arrival of cluster n, $d_{kn} = d_{T,kn} + d_{R,kn}$ is the total travel distance of cluster n estimated as $c\tau_{kn}$, where τ_{kn} is the delay and c is the speed of light.

- since $(x_{C,kn}, y_{C,kn})$ are the coordinates in case of a single reflection, the distance may be chosen uniformly between this point and Tx/Rx location. The new distance from the last or first reflection, depending on which side (Tx or Rx) is considered, is denoted as $d_{u,kn}$;
- compute the coordinate $z_{C,kn}$ as:

- in case of Tx-side, we have:

$$z_{C,kn} = h_T + d_{u,kn} \tan \theta_{D,kn}, \tag{3}$$

- alternatively, in case of Rx-side we have:

$$z_{C,kn} = h_R - d_{u,kn} \tan \theta_{A,kn}, \tag{4}$$

where h_T and h_R are the heights of Tx and Rx k, while $\theta_{D,kn}$ and $\theta_{A,kn}$ are the zenith angles of departure and arrival of cluster n, respectively.

3 MATHEMATICAL FRAMEWORK

In this section, we develop a novel mathematical framework for characterizing the conditional link state probabilities. The considerations below are a comprehensive extension of our previous model in [27] that allow to consider different heights of points O and M. In what follows, we first introduce the preliminary details and then proceed by deriving the unconditional and conditional link state probabilities with respect to the channel with known blockage state. These metrics form the foundation of the proposed spatially-consistent human body blockage state generation procedure for the mmWave channel model introduced in Section 4.

3.1 Important Preliminaries

Consider Fig. 3 illustrating the top-view of the scenario where two clusters are arriving/departing at/from two location points O and M. These clusters are departing/arriving from/at a common point P. In the first case, Tx acts as a common entity located at point P, which is associated with two Rx located at points O and M. In the second case, Rx is considered as a common entity located at point P, which receives two clusters from the reflector points located at O and O and O and O may also be the coordinates of two Tx communicating with a single Rx located at O or, in general, the coordinates of any other nodes.

To establish the conditional link state probability for the general case, we operate with the following terminology: point P with height h_C , point O with height h_1 , and link state (i.e., blocked or non-blocked) derived with unconditional link state probability, as well as point M with height h_2 and link state derived with conditional link state probability. To capture the spatial correlation with respect to the blockage between two links, we are interested in the *conditional link state probabilities* p_{ij} .

Definition 2. p_{ij} , i, j = 0, 1, are the conditional link state probabilities (conditional probabilities) that the state of a node at point M is non-blocked (j = 0) or blocked (j = 1) given that the state of this node at point O is non-blocked (i = 0) or blocked (i = 1), $p_{ij} = \mathbb{P}[M \text{ is in state } j|O \text{ is in state } i]$.

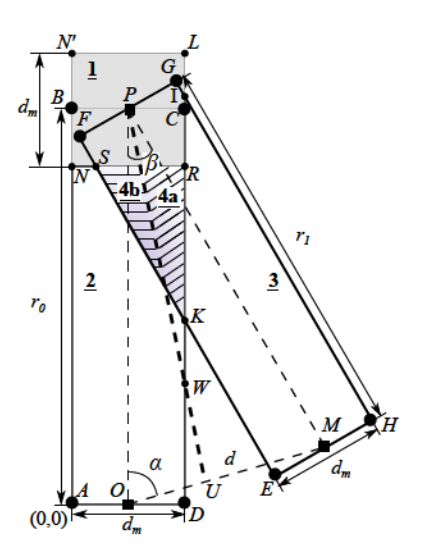


Fig. 3. A top-view illustration of correlation between links.

These probabilities can be organized into the following matrix

$$\mathbf{P} = \begin{pmatrix} p_{00} & p_{01} \\ p_{10} & p_{11} \end{pmatrix} \tag{5}$$

where states 0 and 1 reflect the non-blocked and blocked states, respectively. The matrix **P** is a function of the following variables:

- r_0 is the two-dimensional distance from O to P;
- *d* is the two-dimensional distance from *O* to *M*;
- α is the angle $\angle POM$, see Fig. 3;
- λ_B is the density of blockers;
- h_C, h₁, and h₂ are the heights of points P, O, and M.

Since the following holds [27]

$$p_{00} = 1 - p_{01}, p_{10} = 1 - p_{11},$$
 (6)

in order to parametrize (5), it is required to obtain p_{00} and p_{10} .

The geometry of our proposed methodology is demonstrated in Fig. 3, where two rectangles ABCD and EFGH represent the areas affecting the link PO and PM blockage. The width and length of these rectangles are equal to d_m (the diameter of a blocker) and r_0/r_1 (the 2D distances PO and PM), respectively. One may notice that the intersection area of two rectangles is the area affecting both links PO and PM. For further analysis, the rectangles are divided into multiple zones having a different impact on the conditional probabilities as illustrated in Fig. 3

- Zone 1, NN'LR, is the square area around the point P. Further derivations are simplified significantly by omitting this zone, while the general impact of this zone is considered to be negligible due to its smaller size.
- Zone 2, ANSKD, is related to the path PO and influences the conditional probability in case PO path is blocked.

- **Zone** 3, *IKEH*, affects the *PM* path and does not depend on the state at point *O*.
- Zone 4, SRK, is the common zone affecting both links simultaneously and impacting the dependency between the states at points O and M.

Zone 4 can be split further into two smaller zones, 4a and 4b, which represent the area on the right and left sides, respectively, along with PU, which is the line of intersection of two planes as shown in Fig. 3. These zones are used to determine whether a blocker that is blocking/not blocking the lower plane, is also blocking/not blocking the upper one. Depending on the heights of the involved entities, these zones will correspond to different planes, which is reflected in subsequent derivations.

3.2 Unconditional Link State Probability

We begin with characterizing the unconditional link state probability by deriving it for point O located at the distance of r from point P.

Definition 3. Unconditional link state probability, \mathbb{P}_{nB} , is the probability that a given link is not occluded by a human body, without taking into account the condition of blocked/non-blocked state of the neighboring links.

We follow [26] to briefly sketch the derivation in question. Consider a rectangular blockage zone in Fig. 3 with the width corresponding to the diameter of a blocker, d_m , and the length of r. Recalling that the process associated with the centers of blockers is homogeneous Poisson, the coordinates of each particular blocker are distributed uniformly over $(0,d_m)$ and (0,r), which corresponds to OY and OX coordinates of the rectangle sides, respectively. Hence, the blockage probability is the probability that at least one blocker resides in the area of interest and occludes the link at hand.

For different values of h_C , h_1 , and the distribution of the blocker height H, a blocker falling into the considered area occludes the link when $P\{H > h_m(x)\}$, where $x \in (0,r)$ and $h_m(x)$ is

$$h_m(x) = \frac{h_C - h_1}{r}x + h_1, \ x \in (0, r).$$
 (7)

The non-blocked state probability can now be obtained in terms of the void probability for the PPP as

$$\mathbb{P}_{\mathrm{nB}} = \exp\left[\lambda_B d_m \int_0^r \left(F_H(h_m(x)) - 1\right) dx\right], \quad (8)$$

where $F_H(x)$ is the CDF of the blocker height.

The result in (8) is then employed to derive the conditional link state probabilities. In subsections 3.3, 3.4, and 3.5 we establish the conditional probabilities for the general case, where all of the entities are located at different heights in relation to each other.

$$\mathbb{P}_{nbz} = f_P(0, \lambda_B | S_z) + \sum_{i=1}^{\infty} f_P(i, \lambda_B | S_z) \frac{\left[\sum_{j=1}^{N} \int_{x_j}^{x_{j+1}} \int_{y_j}^{y_{j+1}} F_H\left(\frac{gy - fx - e}{h}\right) | dy | dx \right]^i}{S_z^i}.$$
 (9)

$$\mathbb{P}_{nbz}^* = \exp\left[\lambda_B \sum_{j=1}^N \int_{x_j}^{x_{j+1}} \int_{y_j}^{y_{j+1}} \left[F_H\left(\frac{gy - fx - e}{h}\right) - F_H\left(\frac{by - ax - d}{c}\right) - 1 \right] dy dx \right]. \tag{10}$$

3.3 Probabilities p_{10} and p_{11} for $h_C > h_2$

By observing Fig. 3, one may notice that the planes (ABC) and (EFG) intersect at PU. The zones 4a and 4b are located on the right and left sides of PU, respectively. By using the 3D view of the scenario in Fig. 6, where $h_C > h_2$, we may conclude that the zone 4a of Zone 1, which corresponds to plane (ABC) from Fig. 3, is always higher than the corresponding zone of Zone 2 depicted as plane (EFG). Alternatively, in Fig. 7, when $h_C < h_2$, the zone 4a of Zone 1 is always lower than the zone 4a of plane Zone 2. Therefore, the conditional probabilities are independent of the height h_1 , and it is sufficient to consider two cases, $h_C > h_2$ and $h_C < h_2$.

Let \tilde{L}_z and L_z be the events of having no blockers in zone z that occlude the link paths at O and M, respectively. The complementary events to \tilde{L}_z and L_z are denoted by \tilde{N}_z and N_z . Note that \tilde{L}_z and L_z occur when there are no blockers in zone z or all the blockers are not high enough to occlude the link. When $h_C > h_2$, p_{10} can be written as

$$p_{10} = \frac{\mathbb{P}[M \text{ is non-Blocked} \cap O \text{ is Blocked}]}{\mathbb{P}[O \text{ is Blocked}]}.$$
 (11)

Lemma 1. The probability p_{10} for $h_C > h_2$ given in (11) is simplified to the following form

$$p_{10} = \frac{\mathbb{P}_{nb3} \left(\widetilde{\mathbb{P}}_{b2} \widetilde{\mathbb{P}}_{nb4b} \mathbb{P}_{nb4a} + \mathbb{P}_{nb4b}^* \mathbb{P}_{nb4a} \right)}{1 - \widetilde{\mathbb{P}}_{nb2} \widetilde{\mathbb{P}}_{nb4a} \widetilde{\mathbb{P}}_{nb4b}}, \tag{12}$$

where \mathbb{P}_{nbz} and \mathbb{P}_{bz} are the probabilities of the events L_z and N_z , \mathbb{P}^*_{nb4b} is the probability of $\widetilde{N}_{4b} \cap L_{4b}$, and $\widetilde{\mathbb{P}}_{nbz}$ is the probability of having no blockers affecting the link in the corresponding zone for point O.

Proof: See proof in Appendix A, available in the online supplemental material.

The probabilities \mathbb{P}_{nbz} are derived similarly to the unconditional link state probability in subsection 3.2. They are given by (9), where the auxiliary parameters are provided in Appendix B, available in the online supplemental material, $f_P(i,\lambda_BS_z)$ is the probability of having i blockers in the zone z with the density of blockers λ_B , S_z is the area of zone z, and $F_H([gy-fx-e]/h)$ is the probability that a blocker with the coordinates x, y is lower than the link PM. Note

that here each zone is actually a polygon formed by the intersection of the projections of planes. Since, in fact, (9) integrates over the area of the corresponding zone, it is easier to represent the entire zone as a set of trapezoids and/or triangles with their lower and upper bounds represented as variables x_j, x_{j+1} and y_j, y_{j+1} . The integration limits are provided in our technical report [35].

Using the Maclaurin series expansion of an exponential function, (9) can be simplified as

$$\mathbb{P}_{nbz} = e^{\lambda_B (I - S_z)}. (13)$$

Finally, the probability \mathbb{P}_{nbz} is written as

$$\mathbb{P}_{nbz} = \prod_{j=1}^{N} e^{\lambda_B \int_{x_j}^{x_{j+1}} \int_{y_j}^{y_{j+1}} \left[F_H\left(\frac{gy - fx - e}{h}\right) - 1 \right] dy dx}. \tag{14}$$

Consider now $\widetilde{\mathbb{P}}_{nbz}$, which corresponds to the case where all of the blockers are lower than the plane (ABC). These probabilities are obtained similarly to \mathbb{P}_{nbz} and read as

$$\widetilde{\mathbb{P}}_{nbz} = \prod_{j=1}^{N} e^{\lambda_B \int_{x_j}^{x_{j+1}} \int_{y_j}^{y_{j+1}} \left[F_H\left(\frac{by - ax - d}{c}\right) - 1 \right] dy dx}.$$
(15)

To simplify (12), observe that the following holds

$$\widetilde{\mathbb{P}}_{nb2,4} = \widetilde{\mathbb{P}}_{nb2}\widetilde{\mathbb{P}}_{nb4a}\widetilde{\mathbb{P}}_{nb4b},
\widetilde{\mathbb{P}}_{b2} = 1 - \frac{\widetilde{\mathbb{P}}_{nb2,4}}{\widetilde{\mathbb{P}}_{nb4}},
\widetilde{\mathbb{P}}_{nb4} = \widetilde{\mathbb{P}}_{nb4a}\widetilde{\mathbb{P}}_{nb4b},$$
(16)

where $\mathbb{P}_{nb2,4}$ is the probability of having no blockers in the rectangle ADRN for the link PO. It is calculated by utilizing the generic form (9), which leads to

$$\widetilde{\mathbb{P}}_{nb2,4} = p_0 + \sum_{i=1}^{\infty} p_i \left[\int_{0}^{x_R} \int_{0}^{y_R} \frac{F_H\left[\frac{by - ax - d}{c}\right] dy dx}{||AD||||DR||} \right]^i, \quad (17)$$

where the integration starts at 0, since the point A is located in the center of coordinates.

Finally, using the Maclaurin series expansion of the exponential function, the probabilities \mathbb{P}_{nbz}^* are given by (10), while the integration limits are provided in our technical report [35]. The complementary probability p_{11} is $1 - p_{10}$.

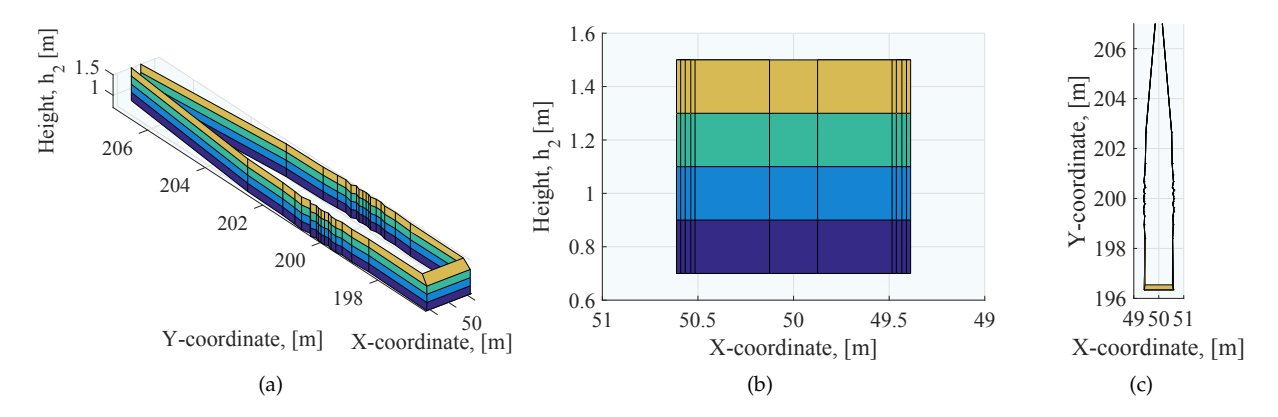


Fig. 4. Illustration of spatially-consistent zone for $h_C = 4$ m, $h_1 = 1.5$ m, and $h_2 \in (0.5 \text{ m} - 1.5 \text{ m})$.

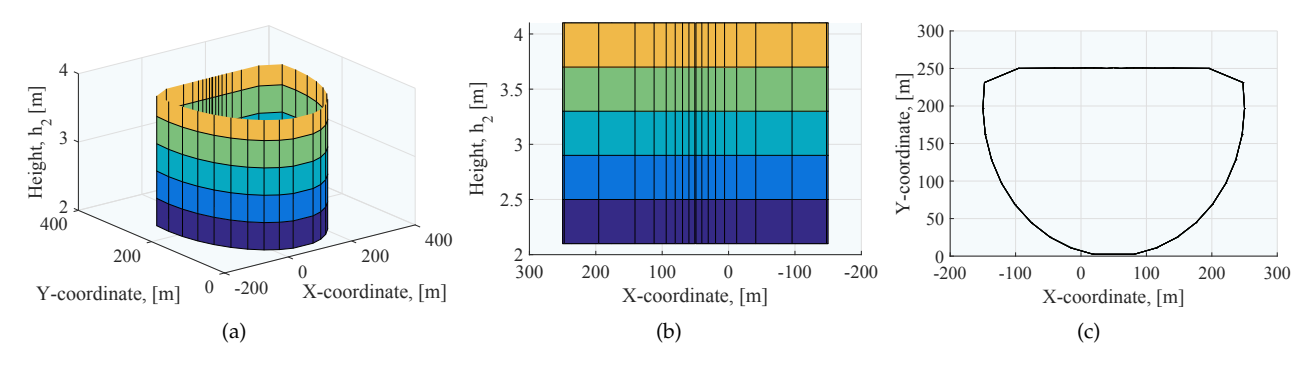


Fig. 5. Illustration of spatially-consistent zone for $h_C = 1.5$ m, $h_1 = 4$ m, and $h_2 \in (2.1 \text{ m} - 4.1 \text{ m})$.

3.4 Probabilities p_{00} and p_{01} for $h_C > h_2$

First, the conditional probability p_{00} can be written as

$$\mathbb{P}\left[M \text{ is non-blocked}|O \text{ is non-blocked}\right] = \frac{\mathbb{P}\left[M \text{ is non-blocked} \cap O \text{ is non-blocked}\right]}{\mathbb{P}\left[O \text{ is non-blocked}\right]}. \tag{18}$$

Note that the event (M is non-blocked) corresponds to the event $L_3 \cap L_{4a} \cap L_{4b}$, while the event (O is non-blocked) corresponds to the event $\widetilde{L}_2 \cap \widetilde{L}_{4a} \cap \widetilde{L}_{4b}$. Observe that zone 4a exists in both planes, while 4a of one plane is always higher than that of another plane. If a blocker in zone 4a is lower for the plane (FGH), it is lower for the upper plane as well; therefore, the following holds: $\widetilde{L}_{4a} \cap L_{4a} = L_{4a}$. The same applies to $\widetilde{L}_{4b} \cap L_{4b} = \widetilde{L}_{4b}$. Hence, (18) can be written as

en as
$$p_{00} = \frac{\mathbb{P}\left[L_3 \cap L_{4a} \cap L_{4b} \cap \widetilde{L}_2 \cap \widetilde{L}_{4a} \cap \widetilde{L}_{4b}\right]}{\mathbb{P}\left[\widetilde{L}_2 \cap \widetilde{L}_{4a} \cap \widetilde{L}_{4b}\right]}$$

$$= \frac{\mathbb{P}\left[L_3 \cap L_{4a}\right]}{\mathbb{P}\left[\widetilde{L}_{4a}\right]}.$$
(19)

Finally, the conditional probability p_{00} can be established as

$$p_{00} = \frac{\mathbb{P}_{nb3}\mathbb{P}_{nb4a}}{\widetilde{\mathbb{P}}_{nb4a}},\tag{20}$$

where \mathbb{P}_{nbz} is the probability of having no blockers in zone z, which is produced by (14), while $\widetilde{\mathbb{P}}_{nbz}$ is

derived in (15). The complementary probability p_{01} is $1 - p_{00}$.

3.5 Conditional Probabilities p_{ij} for $h_C < h_2$

Consider now the case where a common entity height, h_C , is lower than the second entity height, $h_C < h_2$. The analysis in this case is similar to the case of $h_C > h_2$, which has been completed previously, but with one important exception. Here, zones 4a and 4b are located differently with respect to the plane having the non-blocked link path. Hence, we modify (19) for p_{00} as

$$p_{00} = \frac{\mathbb{P}\left[L_3 \cap L_{4b}\right]}{\mathbb{P}\left[\widetilde{L}_{4b}\right]},\tag{21}$$

and the conditional probability p_{00} thus becomes

$$p_{00} = \frac{\mathbb{P}_{nb3}\mathbb{P}_{nb4b}}{\widetilde{\mathbb{P}}_{nb4b}}.$$
 (22)

The complementary probability p_{01} can now be established as $p_{01} = 1 - p_{00}$. Modifying (11) similarly, we arrive at

$$p_{10} = \frac{\mathbb{P}_{nb3} \left(\widetilde{\mathbb{P}}_{b2} \widetilde{\mathbb{P}}_{nb4a} \mathbb{P}_{nb4b} + \mathbb{P}_{nb4a}^* \mathbb{P}_{nb4b} \right)}{1 - \widetilde{\mathbb{P}}_{nb2} \widetilde{\mathbb{P}}_{nb4a} \widetilde{\mathbb{P}}_{nb4b}}.$$
 (23)

The complementary probability p_{11} can now be established as $p_{01} = 1 - p_{10}$.

3.6 Shape of Spatially-Consistent Zone

To assess the effect of correlation caused by human bodies, consider the shape of the *spatially-consistent* (*SpCon*) *zone*.

Definition 4. A spatially consistent zone is the 2D zone around the target node where for every node located inside the SpCon zone the fraction of two conditional link state probabilities, p_{10}/p_{00} , is lower than a value Δx ($\Delta x = 0.99$). Every point at the edge of the SpCon zone coincides with the distance where two conditional probabilities, p_{00} and p_{10} , converge to unconditional probability, \mathbb{P}_{nB} [27]. Any node in the SpCon zone has a spatially consistent blockage state with the target node link state.

The spatially-consistent zone for the case of $h_C=4~\mathrm{m}$ and $h_1=1.5~\mathrm{m}$ as well as the distance between points P and O of $50~\mathrm{m}$, is exemplified in Fig. 4, where the height of point M, h_2 , varies within the range $(0.5,1.5)~\mathrm{m}$. The SpCon zone for the case of $h_C=1.5~\mathrm{m}$ and $h_1=4~\mathrm{m}$ is illustrated in Fig. 5.

As one may observe, the dimensions of the SpCon zone for the second case, $h_C < h_2$, are considerably larger that those for the first case where $h_C > h_2$. To explain this behavior, consider two three-dimensional illustrations for the two considered cases, $h_C > h_2$ and $h_C < h_2$, as displayed in Fig. 6 and Fig. 7, respectively. Here, point P represents the common entity with the height of h_C . Points O and M are the entities with known and unknown states, respectively. All the blockers are smaller than the plane Ω , which is the maximum considered height of a blocker.

Analyzing Fig. 6, which reflects the case of $h_C > h_2$, we note that the area of the zone inducing the correlation between the states is rather small. Indeed, the zone $F_cG_cH_cI_c$ (2D plane in Fig. 6) is the common zone that affects both O and M, while only zone $J_cK_cH_cI_c$ is responsible for the dependence between the states. Most of the common zone is located high enough, where the blockers do not affect the link in question. Hence, the dimension of the SpCon zone in its minor axis is very small, since an increase in the distance between points O and M decreases the intersection area.

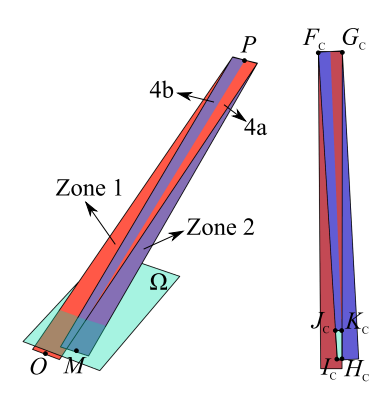


Fig. 6. Illustration of the case $h_C > h_2$.

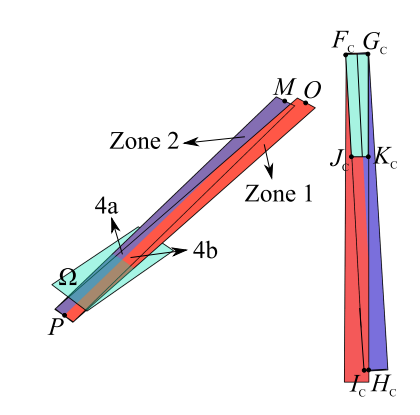


Fig. 7. Illustration of the case $h_C < h_2$.

In Fig. 7, the zone $F_cG_cH_cI_c$ (2D plane in Fig. 7) is the common zone that affects both O and M. Here, only zone $F_cG_cJ_cK_c$ is responsible for the dependence between the states. Hence, an increase in the distance between the two entities maintains the correlation farther than in the first case.

4 SPATIALLY-CONSISTENT BLOCKAGE STATE GENERATION PROCEDURE

After obtaining the unconditional and conditional link state probabilities, we proceed with specifying a spatially-consistent blockage state generation procedure for micro objects (human bodies). Our proposed procedure can be overlaid on top of the standard 3GPP channel model or on top of any 3GPP-like channel models.

The main goal of the proposed procedure is to assign the spatially consistent blocked/non-blocked state to every link in a given scenario. Algorithm 1 is responsible for generating blocked/non-blocked states among all the Tx-Rx links, whereas Algorithm 2 is responsible for generating blocked/non-blocked states among all the Reflector-Rx links. Both algorithms employ our analytical framework to derive the conditional link state probabilities given in Section 3. The computation complexity of the algorithms grows linearly with the number of Rx nodes i.e., the overall modeling complexity is O(K), where K is the number of Rx generated in the scenario. Note that the algorithms do not depend on the blocker density, since this density is a parameter of the analytical framework.

The proposed state generation procedure comprises three phases. At the first phase, we associate every Rx with the state (blocked/non-blocked) of the LoS path. First, we generate K Rx with uniformly distributed x- and y-coordinates. Further, we introduce two sets, $N_{\rm U1}$ and $N_{\rm U2}$, containing the coordinates of Rx without and with generated blockage states. The set $N_{\rm U,s}$ contains blockage states of LoS links for all Rx. Further, we choose the first Rx from the set $N_{\rm U1}$ and find the unconditional state of that Rx by using the unconditional link state probability, $\mathbb{P}_{\rm nB}$, from (8). We

Algorithm 1: Blocked/non-blocked LoS state generation

Result: Blocked/non-blocked LoS states for all Rx

- 1 Generate uniformly distributed coordinates $(x_{R,1},y_{R,1}),\ldots,(x_{R,K},y_{R,K})$ of K Rx
- 2 Define the sets $N_{\rm U1} = \emptyset$ and $N_{\rm U2} = \emptyset$ for the coordinates of Rx w/o and w/ blocked/non-blocked state, respectively
- 3 Define the set $N_{\text{U,s}} = \emptyset$ for blocked/non-blocked states of every Rx
- 4 Save the coordinates of every Rx to the set $N_{\text{U1}} = \{(x_{R,1}, y_{R,1}), \dots, (x_{R,K}, y_{R,K})\}$

5 while $N_{U1} \neq \emptyset$ do

8

10

12

13

14

15

16

17

18

19

20

Choose the coordinates of Rx k from the set $N_{\rm U1}$ Find the unconditional state $q_{u,k}^R = \{0 \text{ or } 1\}$ of Rx k based on the unconditional probability, $\mathbb{P}_{\rm nB}$, from (8)

Save the state of Rx k to the set $N_{\text{U,s}} = N_{\text{U,s}} \cup q_{u,k}^R$ Remove the coordinates of Rx k from the set N_{U1} Add the coordinates of Rx k to the set

 $N_{U2} = N_{U2} \cup (x_{R,k}, y_{R,k})$

11 while $N_{U2} \neq \emptyset$ do

Choose the coordinates of Rx l from the set $N_{\rm U2}$ Calculate the SpCon zone (see Definition 4) for Rx l using the conditional probabilities, $p_{\rm 10}$ from (12), $p_{\rm 00}$ from (20), and the unconditional probability, $\mathbb{P}_{\rm nB}$ from (8) Remove the coordinates of Rx l from $N_{\rm U2}$ Find any Rx from the set $N_{\rm U1}$ in the SpCone zone of Rx l

if $Rx \ m$ from the set N_{UI} is in the SpCone zone then

Find the conditional state $q_{c,m}^R = \{0 \text{ or } 1\}$ of Rx m using (12) or (20) Add the coordinates of Rx m to the set $N_{U2} = N_{U2} \cup (x_{R,m}, y_{R,m})$

Save the state of Rx m to the set $N_{\mathrm{U,s}} = N_{\mathrm{U,s}} \cup q_{c,m}^R$

Remove the coordinates of Rx m from the set $N_{\rm U1}$

continue by calculating the SpCon zone for the first selected Rx by following the Definition 4. All of the Rx that fall into the SpCon zone have the correlated link states with the link state of a chosen Rx. In case where no Rx are in the SpCone zone, the next Rx from the set $N_{\rm U1}$ is selected and the procedure repeats. The generation procedure continues up until all the Rx are assigned with blocked/non-blocked LoS states.

At the second phase, we generate the cluster channel parameters (AoA, AoD, ZoA, ZoD, and delay) for every Rx by following the 3GPP channel model generation procedure [21]. Finally, at the last phase, the state of each cluster for every Rx is generated. The set $N_{\rm C}$ contains the aforementioned cluster channel parameters of all clusters for all the Rx. The sets $N_{\rm Ck1}$ and $N_{\rm Ck2}$ contain cluster coordinates without and with blocked/non-blocked states. The set $N_{\rm Ck,s}$ contains the states of every cluster for each Rx in the scenario. We choose the first cluster of Rx $k=(1,\ldots,K)$ and find the state by using the unconditional probability, $\mathbb{P}_{\rm nB}$,

Algorithm 2: Blocked/non-blocked link state generation for every cluster of each Rx

Result: Blocked/non-blocked states for all clusters

- 1 Generate the cluster channel parameters $(\phi_{A,kn},\phi_{D,kn},\theta_{A,kn},\theta_{D,kn}, au_{kn})$ for all K Rx [9]
- 2 Define the set $N_C = \emptyset$ for the parameters of clusters for every Rx w/o state
- ³ Define the set $N_{\text{Ck,s}} = \emptyset$ for the blocked/non-blocked states of every cluster for each Rx
- 4 Add all the parameters of clusters for each Rx to the set $N_{\rm C} = (\phi_{A,kn}, \phi_{D,kn}, \theta_{A,kn}, \theta_{D,kn}, \tau_{kn})$

while $N_C \neq \emptyset$ do

Choose the parameters of clusters for Rx k from the set $N_{\rm C}$

Find $x_{C,kn}$, $y_{C,kn}$, and $z_{C,kn}$ coordinates of clusters $n=1,\ldots,N$, see Section 2.3

8 Remove the parameters of clusters for Rx k from the set $N_{\rm C}$

Define the sets $N_{\text{Ck1}} = \emptyset$ and $N_{\text{Ck2}} = \emptyset$ for the coordinates of clusters for Rx k, w/o and w/ state respectively

Add the coordinates of clusters for Rx k to the set $N_{\text{Ck1}} = \{(x_{C,k1}, y_{C,k1}, z_{C,k1}), \dots, (x_{C,kN}, y_{C,kN}, z_{C,kN})\}$

11 while $N_{Ck1} \neq \emptyset$ do

12

13

14

15

16

17

18

19

20

24

Choose the coordinates of cluster l from the set N_{Ck1}

Find the unconditional state $q_{u,l}^C = \{0 \text{ or } 1\}$ of cluster l based on the unconditional probability, \mathbb{P}_{nB} , from (8)

Save the state of cluster l to the set

 $N_{\text{Ck,s}} = N_{\text{Ck,s}} \cup q_{u,l}^C$

Add the coordinates of cluster l to the set

 $N_{\text{Ck2}} = N_{\text{Ck2}} \cup (x_{C,kl}, y_{C,kl}, z_{C,kl})$

Remove the coordinates of cluster l from the set $N_{\rm Ck1}$

while $N_{Ck2} \neq \emptyset$ do

Choose the coordinates of cluster e from the set $N_{\rm Ck2}$

Find the conditional probabilities p_{10} and p_{00} for the link state of cluster m from the set $N_{\rm Ck1}$

Remove the coordinates of cluster e from the set $N_{\rm Ck2}$

if $p_{10}/p_{00} < 0.99$ then

Find the conditional state

 $q_{c,m}^C = \{0 \text{ or } 1\}$ of the cluster m based on the conditional probabilities p_{10} or p_{00}

Save the state of cluster m to the set

 $N_{\text{Ck,s}} = N_{\text{Ck,s}} \cup q_{c,m}^C$

Add the coordinates of cluster m to the set $N_{\rm Ck2}$

Remove the coordinates of cluster m from the set $N_{\rm Ck1}$

(8). Due to different heights of the arrived clusters, there is no common 2D SpCon zone for a given cluster reflection point. Therefore, the rest of the clusters without the link states are compared individually with the chosen cluster to identify any correlated links among the clusters. Any chosen cluster is considered

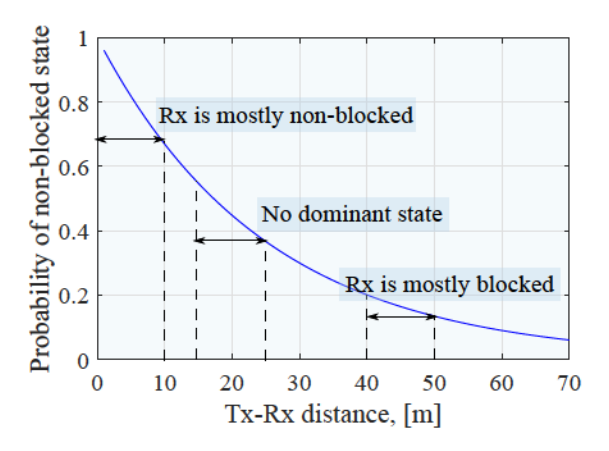


Fig. 8. Unconditional probability, \mathbb{P}_{nB} , of non-blocked state, $\lambda_B = 1$.

to have a correlated link state with the link state of cluster 1 if the fraction of two conditional link state probabilities, p_{10}/p_{00} , is lower than a certain value Δx ($\Delta x = 0.99$). The conditional state probabilities p_{10} and p_{00} are calculated based on (12)/(23) and (20)/(21) by taking into account the heights of the considered clusters and the Rx. The generation procedure continues up until all the clusters of all the Rx are assigned with blocked/non-blocked states.

The pseudo code for the above phases is provided in Algorithms 1 and 2, where Algorithm 1 covers the first phase, while Algorithm 2 implements the second and third phases.

5 Key Numerical Results

In this section, we illustrate the performance of the generation procedure as well as study the effects of correlation caused by micro objects (human bodies) in the mmWave channel, which we compare with the case of no correlation among the links. We consider a crowded environment, where the density of blockers in the modeled area is $\lambda_B = 1$ blockers per square meter. The height of Tx is 4 m and the height of each Rx is 1.5 m. The Tx is located at the origin (0,0), while K Rx are distributed uniformly within the area of interest. The received power of every Rx is established by using the 3GPP urban micro (UMi) street canyon path loss model and the cluster based channel model [9]. In case the link is blocked, we assume 20 dB loss [36]. The link blockage state is derived by employing our spatially-consistent human body blockage state generation algorithm as well as independent generation of the link blockage states. The remaining parameters are collected in Table 2.

Let the coordinates of K Rx be uniformly distributed in three different areas of 10 by 10 square meters. The left bottom edges of these areas are located at $(x_{L,B}, y_{L,B})$ coordinates of (1,1), (15,15), and (40,40) referring to the different 2D separation distances between the Tx and the closest Rx. These

coordinates where chosen to study the impact of the most probable link state in three different cases: (i) Rx are mostly in non-blocked state (probability of non-blocked state is about 0.8 in Fig. 8); (ii) there is no dominant state (probability of non-blocked state is about 0.5 in Fig. 8), and (iii) Rx are mostly in blocked state (probability of non-blocked state is about 0.2 in Fig. 8). Below, we formulate our key findings in terms of important statements.

We first compare the output of our algorithms with the data of our simulator [30], where blockers were modeled explicitly. We model blockers as cylinders with the density of $\lambda_B=1$ blockers per square meter for the scenario described above. In Fig. 9(b), it may be observed that the simulation results match closely the ones derived with the proposed algorithm. A slight mismatch between the data sets is explained by the assumption of the analytical model, where the blocker occludes the link if its height is lower than the LoS link at the point, where the blocker's center is located. In the simulator, the blocker might still block the path with its edge in some cases.

Observation 1: Spatial consistency across the blockage states of the links does not impact the mean received power averaged over large area of interest but affects the received power of the neighboring links. Fig. 9 demonstrates the CDFs of the received power, P_R , for three different assumptions regarding the blockage state generation: (i) no blockers (all the Rx are in LoS); (ii) uncorrelated blockage states; (iii) correlated blockage states for three different positions of the left bottom edge of the Rx distribution area of 10 m \times 10 m: (1,1), (15,15), and (40,40). Here, the number of Rx, K, was set to 100. As one may observe in Fig. 9, the CDFs of the received power coincide for the scenarios with correlated and uncorrelated blockage states. The reason is that the received power averaged across all of the Rx distributed in the area larger than the SpCon zone of one Rx remains the same on average. However, if we consider the area that is much smaller than the SpCon zone of one Rx, e.g., 1 m×1 m, the difference in the CDFs of the received power for correlated and uncorrelated blockage states becomes noticeable as confirmed in

TABLE 2
Baseline system parameters

Parameter	Value
Height of Tx, h_T	4 m
Height of Rx, h_R	1.5 m
Height of a blocker, $N(\mu_H, \sigma_H)$	N(1.7 m, 0.1 m)
Diameter of a blocker, d_m	0.5 m
Coordinates of the left bottom edge of the area	(1,1), (15,15),
with distributed K Rx, $(x_{L,B}, y_{L,B})$	and (40, 40)
Density of blockers, λ_B	1 bl/m^2
Carrier frequency	28 GHz
Transmit power	35 dBm
Blockage penalty	20 dB
Number of clusters, N	5

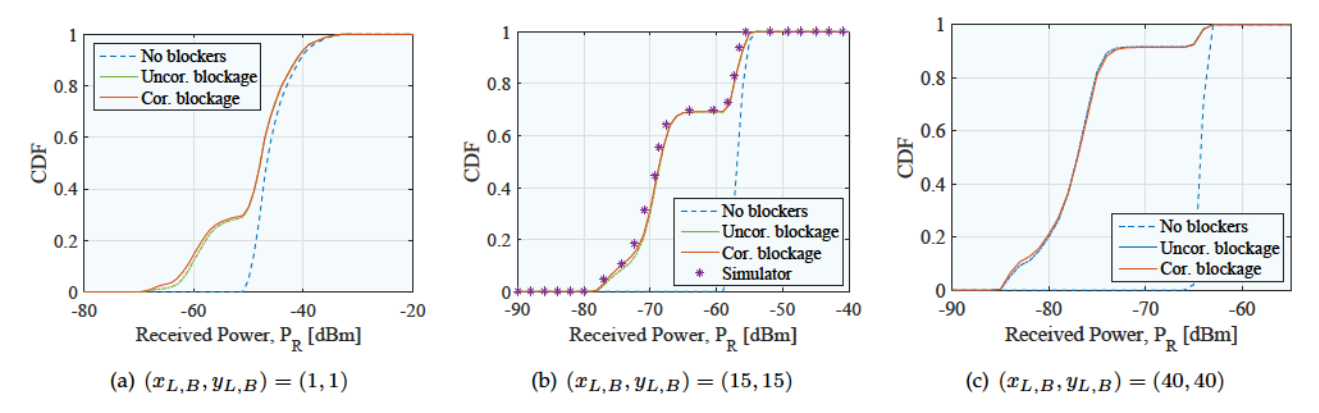


Fig. 9. Received power CDF: 100 Rx distributed in 10 m×10 m area.

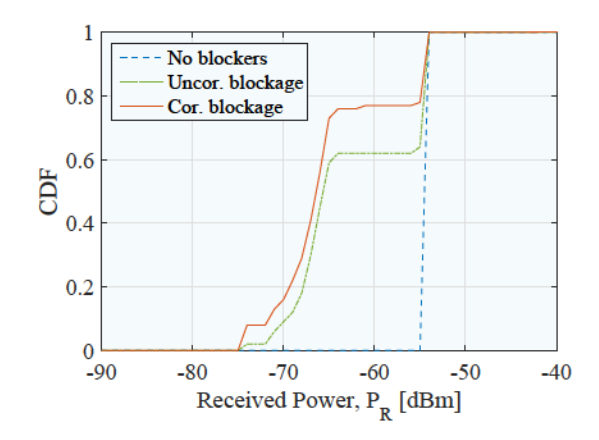
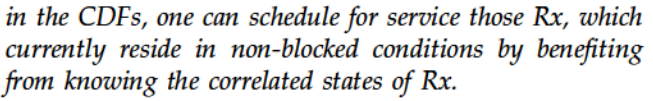


Fig. 10. Received power CDF: 100 Rx, 1 m×1 m area, $(x_{L,B}, y_{L,B}) = (15, 15)$.

Fig. 10. It is explained by the fact that most of the Rx are falling into the SpCon zone of one Rx, so that all the links are correlated with each other. Therefore, the correlation across the blockage states highly affects the performance of the neighboring links.

However, note that these results do not imply that the knowledge of correlated states of receivers cannot improve the system performance. Even though there is no difference



Observation 2: Increased density of Rx leads to an increased number of correlated links. The effect of Rx density on the proportion of correlated links is demonstrated in Fig. 11 and Fig. 12, where the total numbers of Rx per 10 m \times 10 m area are 20 and 100, respectively. The plots illustrate the difference in the received power calculated for the same set of Rx but with different blockage state generation procedure: (i) correlated blockage states and (ii) uncorrelated blockage states. The figures reflect only those Rx, which see a difference in the received power. The positions of the small squares in the plots represent the aforementioned Rx locations and the color of the squares demonstrates the absolute power difference. It is observed that for one particular realization of the field of Rx displayed in the plots the percentage of receivers with correlated link states increases from 45% among 20 Rx to 97\% Rx among 100 Rx in 10 m×10 m area.

However, the number of Rx with different received power is significantly smaller referring to the 10% among 20 Rx and 16% among 100 Rx. The reason

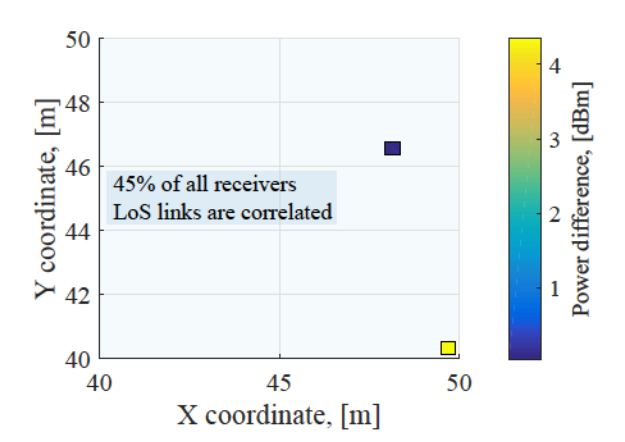


Fig. 11. Number of correlated receivers among 20 Rx in 10 m×10 m area, $(x_{L,B},y_{L,B})=(40,40)$.

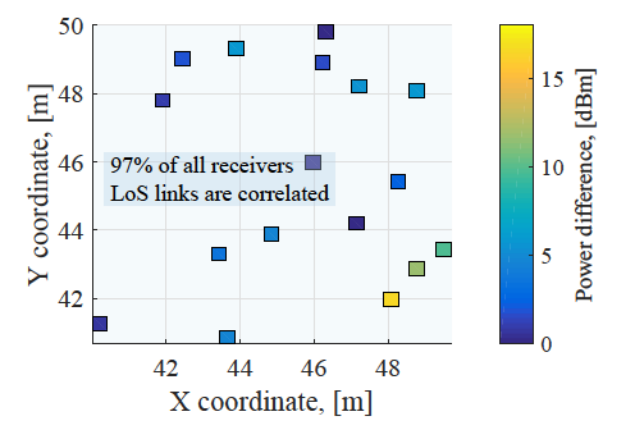


Fig. 12. Number of correlated receivers among 100 Rx in 10 m×10 m area, $(x_{L,B},y_{L,B})=(40,40)$.

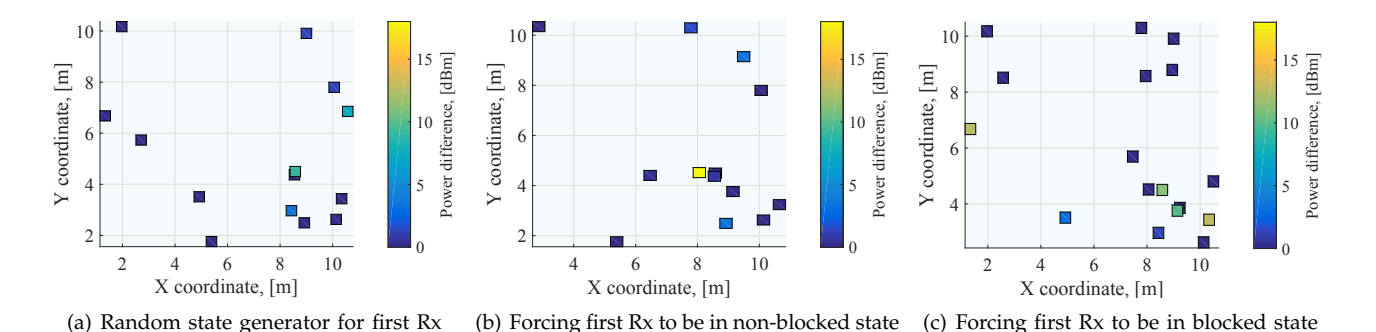
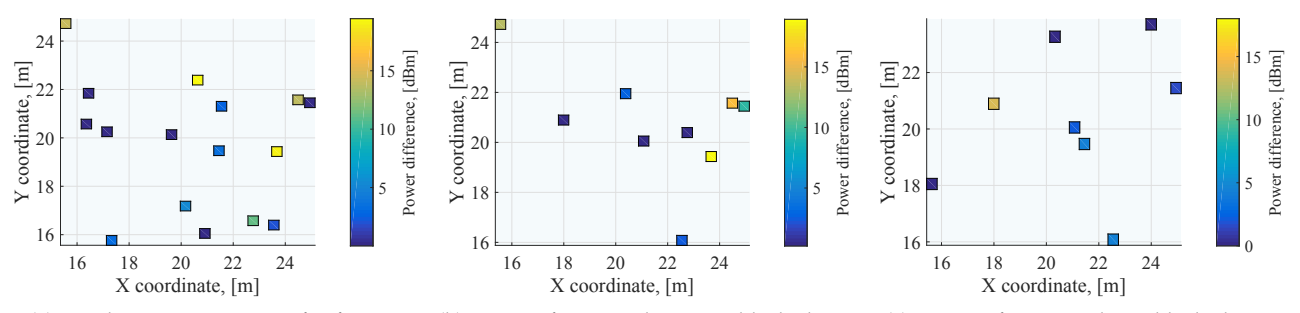


Fig. 13. Absolute received power difference between correlated and uncorrelated blockage state generation for 50 Rx, $(x_{L,B}, y_{L,B}) = (1,1)$.



(a) Random state generator for first Rx (b) Forcing first Rx to be in non-blocked state (c) Forcing first Rx to be in blocked state

Fig. 14. Absolute received power difference between correlated and uncorrelated blockage state generation for 50 Rx, $(x_{L,B}, y_{L,B}) = (15, 15)$.

is that there is a number of Rx, which are assigned a blocked/non-blocked state based on the unconditional probability in the spatially consistent blockage state generation procedure. For high unconditional blockage probability, these states will most probably be blocked states. The receivers that are located in the SpCon zone of the Rx with unconditional blockage states having a high probability will follow the link state of the latter Rx. Therefore, the number of Rx with different received power is low, since most of the Rx will be assigned the most probable link state.

Observation 3: The difference between received power calculated with the help of the correlated and uncorrelated state generation procedures in a single realization increases when the first chosen Rx is assigned a less probable state (e.g., the unconditional non-blockage probability is 0.8, but with the probability 0.2 the Rx could be assigned the blocked state, which is a less probable state). It was noted in the previous plots that the number of Rx with different received power for two different blockage state generation cases (conditional and unconditional) is rather small, since the Rx is assigned the most probable link states. With Fig. 13 and Fig. 14, we study the effect of the link state that deviates from the most probable case. For the three subplots in Fig. 13, a set of 50 Rx was generated once in the 10 m×10 m area with the left bottom coordinates $(x_{L,B},y_{L,B})=(1,1)$. The small squares refer to the positions of Rx with different received power for the correlated and uncorrelated blockage state generation cases. Also, the position of every Rx is the same for each subplot of Fig. 13. The first Rx chosen by the spatially consistent blockage state generation procedure is assigned a blockage state following three different strategies: (i) the first chosen Rx is assigned a blockage state based on the unconditional probability; (ii) the first chosen Rx is assigned a non-blocked state; (iii) the first chosen Rx is assigned a blocked state. The latter strategies were chosen to study the effect of a single link state.

It was observed that the number of Rx with different received power for the two scenarios (unconditional and conditional blockage state generation cases) increases when the first chosen Rx is assigned a less probable state. For Fig. 13, this state is the blocked state, since the unconditional non-blockage probability is about 0.8. To further demonstrate the effect of the most probable state of the Rx, we generate 50 Rx in the area of 10 m×10 m area with $(x_{L,B}, y_{L,B}) = (15, 15)$; the results are depicted in Fig. 14. These coordinates were chosen, since there is no most probable state of the Rx (unconditional blockage probability is around 0.5). The results indicate no major difference between the number of Rx with different received power when assigning the first Rx with a blocked or non-blocked state.

6 Conclusions

In this paper, we proposed a new 3GPP-compatible spatially-consistent human body blockage state generation procedure for dense urban mmWave deployments. The contributed model is built on top of a globally accepted 3GPP model and extends it to the case of correlated signal behavior caused by a human crowd around the mmWave receivers. We also investigated in detail the effects of correlation created by human bodies to demonstrate that it manifests itself in a local fluctuation of the received signal strength as well as heavily depends on the density of the receivers. The main application area for the proposed state generation procedure is in systemlevel simulations of the emerging cellular mmWave technology. In this setting, our model can be used as an extension to the 3GPP's model with correlated macro objects, thus inducing additional dependency in the received signal strength field caused by the human crowd. The computational complexity of our model does not depend on the blocker density, which makes it suitable for characterizing densely crowded environments.

REFERENCES

- [1] ITU-R, "IMT vision framework and overall objectives of the future development of IMT for 2020 and beyond," Recommendation ITU-R M.2083-0, September 2015.
- [2] J. G. Andrews, S. Buzzi, C. Wan, S. V. Hanly, A. Lozano, A. C. K. Soong, and J. C. Zhang, "What will 5G be?" *IEEE Journal on Selected Areas in Communications*, vol. 32, no. 6, pp. 1065–1082, June 2014.
- [3] A. Ghosh, T. A. Thomas, M. C. Cudak, R. Ratasuk, P. Moorut, F. W. Vook, T. S. Rappaport, G. R. MacCartney, S. Sun, and S. Nie, "Millimeter-wave enhanced local area systems: A highdata-rate approach for future wireless networks," *IEEE Journal* on Selected Areas in Communications, vol. 32, no. 6, pp. 1152– 1163, June 2014.
- [4] J. G. Andrews, T. Bai, M. N. Kulkarni, A. Alkhateeb, A. K. Gupta, and R. W. Heath, "Modeling and analyzing millimeter wave cellular systems," *IEEE Transactions on Communications*, vol. 65, no. 1, pp. 403–430, January 2017.
- [5] M. Gapeyenko, V. Petrov, D. Moltchanov, S. Andreev, N. Himayat, and Y. Koucheryavy, "Flexible and reliable UAV-assisted backhaul operation in 5G mmWave cellular networks," *IEEE Journal on Selected Areas in Communications*, vol. 36, no. 11, pp. 2486–2496, November 2018.
- [6] M. Abouelseoud and G. Charlton, "The effect of human blockage on the performance of millimeter-wave access link for outdoor coverage," in *IEEE Vehicular Technology Conference* (VTC Spring), June 2013, pp. 1–5.
- [7] M. N. Kulkarni, A. O. Kaya, D. Calin, and J. G. Andrews, "Impact of humans on the design and performance of millimeter wave cellular networks in stadiums," in *IEEE Wireless Communications and Networking Conference (WCNC)*, March 2017, pp. 1–6.
- [8] T. Wu, T. S. Rappaport, and C. M. Collins, "The human body and millimeter-wave wireless communication systems: Interactions and implications," in *IEEE International Conference* on Communications (ICC), June 2015, pp. 2423–2429.
- [9] 3GPP, "Study on channel model for frequencies from 0.5 to 100 GHz (Release 15)," 3GPP TR 38.901 V15.0.0, June 2018.
- [10] METIS, "Initial channel models based on measurements," METIS deliverable D1.2, April 2014.
- [11] T. A. Thomas, H. C. Nguyen, and G. R. MacCartney, "3D mmWave channel model proposal," in *IEEE Vehicular Tech*nology Conference (VTC Fall), September 2014, pp. 1–6.

- [12] M. Zhang, M. Mezzavilla, R. Ford, S. Rangan, S. Panwar, E. Mellios, D. Kong, A. Nix, and M. Zorzi, "Transport layer performance in 5G mmwave cellular," in 2016 IEEE Conference on Computer Communications Workshops (INFOCOM WKSHPS), April 2016, pp. 730–735.
- [13] M. Gapeyenko, V. Petrov, D. Moltchanov, S. Andreev, Y. Koucheryavy, M. Valkama, M. R. Akdeniz, and N. Himayat, "An analytical representation of the 3GPP 3D channel model parameters for mmWave bands," in 2nd ACM Workshop on Millimeter-Wave Networks and Sensing Systems, October 2018, pp. 1–6.
- [14] F. Baccelli and X. Zhang, "A correlated shadowing model for urban wireless networks," in *IEEE Conference on Computer Communications (INFOCOM)*, August 2015, pp. 801–809.
- [15] S. Sun, H. Yan, G. R. MacCartney, and T. S. Rappaport, "Millimeter wave small-scale spatial statistics in an urban microcell scenario," in *IEEE International Conference on Communications* (ICC), May 2017, pp. 1–7.
- [16] C. S. Choi, J. O. Woo, and J. G. Andrews, "On the coverage probability of a spatially correlated network," in *IEEE Inter*national Symposium on Information Theory (ISIT), June 2017, pp. 466–470.
- [17] G. R. MacCartney, M. K. Samimi, and T. S. Rappaport, "Exploiting directionality for millimeter-wave wireless system improvement," in *IEEE International Conference on Communications* (ICC), June 2015, pp. 2416–2422.
- [18] M. N. Kulkarni, A. Ghosh, and J. G. Andrews, "A comparison of MIMO techniques in downlink millimeter wave cellular networks with hybrid beamforming," *IEEE Transactions on Communications*, vol. 64, no. 5, pp. 1952–1967, May 2016.
- [19] A. K. Gupta, J. G. Andrews, and R. W. Heath, "Macrodiversity in cellular networks with random blockages," *IEEE Transac*tions on Wireless Communications, vol. 17, no. 2, pp. 996–1010, February 2018.
- [20] V. Va, J. Choi, and R. W. Heath, "The impact of beamwidth on temporal channel variation in vehicular channels and its implications," *IEEE Transactions on Vehicular Technology*, vol. 66, no. 6, pp. 5014–5029, June 2017.
- [21] Nokia et al., "5G channel model for bands up to 100 GHz," 5GCM white paper available at: http://www.5gworkshops.com, October 2016.
- [22] A. Molisch, A. Karttunen, S. Hur, J. Park, and J. Zhang, "Spatially consistent pathloss modeling for millimeter-wave channels in urban environments," in *Proc. Eur. Conf. Antennas Propag.(EuCAP)*, pp. 1–5.
- [23] A. Karttunen, A. F. Molisch, S. Hur, J. Park, and C. J. Zhang, "Spatially consistent street-by-street path loss model for 28-GHz channels in micro cell urban environments," *IEEE Transactions on Wireless Communications*, vol. 16, no. 11, pp. 7538–7550, November 2017.
- [24] S. Ju and T. S. Rappaport, "Simulating motion incorporating spatial consistency into the NYUSIM channel model," in *IEEE 88th Vehicular Technology Conference (VTC Fall)*, August 2018, pp. 1–6.
- [25] T. Bai, R. Vaze, and R. W. Heath, "Analysis of blockage effects on urban cellular networks," *IEEE Transactions on Wireless Communications*, vol. 13, no. 9, pp. 5070–5083, September 2014.
- [26] M. Gapeyenko, A. Samuylov, M. Gerasimenko, D. Moltchanov, S. Singh, E. Aryafar, S.-p. Yeh, N. Himayat, S. Andreev, and Y. Koucheryavy, "Analysis of human-body blockage in urban millimeter-wave cellular communications," in 2016 IEEE International Conference on Communications (ICC). IEEE, May 2016, pp. 1–7.
- [27] A. Samuylov, M. Gapeyenko, D. Moltchanov, M. Gerasimenko, S. Singh, N. Himayat, S. Andreev, and Y. Koucheryavy, "Characterizing spatial correlation of blockage statistics in urban mmWave systems," in *IEEE Global Communications Workshops* (GLOBECOM Wkshps), December 2016, pp. 1–7.
- [28] G. R. MacCartney, T. S. Rappaport, and A. Ghosh, "Base station diversity propagation measurements at 73 GHz millimeter-wave for 5G coordinated multipoint (CoMP) analysis," in *IEEE Global Communications Workshops (GLOBECOM Wkshps)*, December 2017, pp. 1–7.
- [29] S. Aditya, A. F. Molisch, N. Rabeah, and H. M. Behairy, "Localization of multiple targets with identical radar signatures in multipath environments with correlated blocking," *IEEE*

Transactions on Wireless Communications, vol. 17, no. 1, pp. 606–618, January 2018.

[30] "WINTERsim system-level simulator, 2015," http://winter-group.net/downloads/.

[31] M. Jacob, S. Priebe, T. Kurner, M. Peter, M. Wisotzki, R. Felbecker, and W. Keusgen, "Fundamental analyses of 60 GHz human blockage," in *Proc. of European Conference on Antennas and Propagation (EuCAP)*, April 2013, pp. 117–121.

[32] C. L. Ogden, C. D. Fryar, M. D. Carroll, and K. M. Flegal, "Mean body weight, height, and body mass index, United States 1960–2002," Centers for Disease control and prevention, no. 347, October 2004.

[33] 3GPP, "Study on 3D channel model for LTE (release 12)," TR 36.873 V12.7.0, January 2018.

[34] —, "Winner II channel models," IST-4-027756 WINNER II, D1.1.2 V1.2, 2008.

[35] A. Samuylov *et al.*, "Characterizing spatial correlation of blockage statistics," Tampere University of Technology, Technical report available at: http://winter-group.net/downloads/mmWave_blockage_report.pdf, 2016.
 [36] K. Haneda *et al.*, "5G 3GPP-like channel models for outdoor

[36] K. Haneda et al., "5G 3GPP-like channel models for outdoor urban microcellular and macrocellular environments," in IEEE 83rd Vehicular Technology Conference (VTC Spring), May 2016, pp. 1–7.



Mikhail Gerasimenko is a Researcher at Tampere University in the Laboratory of Electronics and Communications Engineering. Mikhail received Specialist degree from Saint-Petersburg University of Telecommunications in 2011. In 2013, he obtained Master of Science degree from TUT. In 2018 he also obtained Doctor of Science degree from Tampere University of Technology. Mikhail started his academic career in 2011 and since then he appeared as (co-)author of

multiple scientific journal and conference publications, as well as several patents. He also acted as reviewer and participated in educational activities. His main subjects of interest are wireless communications, machine-type communications, and heterogeneous networks.



Dmitri Moltchanov is a Senior Research Scientist in the Laboratory of Electronics and Communications Engineering, Tampere University, Finland. He received his M.Sc. and Cand.Sc. degrees from Saint-Petersburg State University of Telecommunications, Russia, in 2000 and 2002, respectively, and Ph.D. degree from Tampere University of Technology in 2006. His research interests include performance evaluation and optimization issues of wired and wireless IP

networks, Internet traffic dynamics, quality of user experience of real-time applications, and traffic localization P2P networks. Dmitri Moltchanov serves as TPC member in a number of international conferences. He authored more than 80 publications.



Margarita Gapeyenko is a Ph.D. candidate at the Laboratory of Electronics and Communications Engineering at Tampere University, Finland. She earned her M.Sc. degree in Telecommunication Engineering from University of Vaasa, Finland, in 2014, and B.Sc. degree in Radio-Engineering, Electronics, and Telecommunications from Karaganda State Technical University, Kazakhstan, in 2012. Her research interests include mathematical analysis, performance evaluation,

and optimization methods of future wireless networks, device-todevice communication, and 5G-grade heterogeneous networks.



Sarabjot Singh ('SM 09, M' 15) is a Principal Engineer at Uhana Inc. CA. He received the B. Tech. from IIT, India, and the M.S.E and Ph.D. in EE from UT Austin. His past affiliations include Intel, Nokia Technologies, Bell Labs, and Qualcomm Inc, where he worked on protocol and algorithm design for next generation of cellular and WiFi networks. Dr. Singh is interested in the system and architecture design of wireless networks leveraging theoretical and applied tools. He is a co-

author of more than 40 patent applications, and multiple conference and journal papers. He was the recipient of the President of India Gold Medal in 2010, the ICC Best Paper Award in 2013, and recognized for being a prolific inventor at Intel Corp.



Andrey Samuylov received the Ms.C. in Applied Mathematics and Cand.Sc. in Physics and Mathematics from the RUDN University, Russia, in 2012 and 2015, respectively. Since 2015 he is working at Tampere University as a researcher, focusing on mathematical performance analysis of various 5G wireless networks technologies. His research interests include P2P networks performance analysis, performance evaluation of wireless networks with enabled D2D communications,



Mustafa Riza Akdeniz (S'09) received the B.S. degree in electrical and electronics engineering from Bogazici University, Istanbul, Turkey, in 2010 and the Ph.D. degree in electrical and computer engineering at New York University Tandon School of Engineering, Brooklyn, NY in 2016. He is working as a research scientist for Intel Labs in Santa Clara, CA. His research interests include wireless communications, wireless channel modeling, and information theory.

and mmWave band communications.



Ehsan Aryafar is an Assistant Professor of Computer Science at Portland State University. Prior to that and from 2013 to 2017, he was a Research Scientist at Intel Labs in Santa Clara, CA. He received the B.S. degree in Electrical Engineering from Sharif University of Technology, Iran, in 2005, and the M.S. and Ph.D. degrees in Electrical and Computer Engineering from Rice University, Houston, Texas, in 2007 and 2011, respectively. From 2011 to 2013, he was a Post-

Doctoral Research Associate in the Department of Electrical Engineering at Princeton University. His research interests are in the areas of wireless networks and networked systems, and span both algorithm design as well as system prototyping. He has more than 30 issued and pending patents in the areas of mobile and wireless systems.



Sergey Andreev is a Professor in the Laboratory of Electronics and Communications Engineering at Tampere University, Finland. He received the Specialist degree (2006) and the Cand.Sc. degree (2009) both from St. Petersburg State University of Aerospace Instrumentation, St. Petersburg, Russia, as well as the Ph.D. degree (2012) from Tampere University of Technology. Sergey (co)authored more than 100 published research works on wireless communications, energy

efficiency, heterogeneous networking, cooperative communications, and machine-to-machine applications.



Nageen Himayat is a Principal Engineer with Intel Labs, where she leads a team conducting research on several aspects of next generation (5G/5G+) of mobile broadband systems. Her research contributions span areas such as multi-radio heterogeneous networks, mm-wave communication, energy-efficient designs, cross layer radio resource management, multi-antenna, and non-linear signal processing techniques. She has authored over 250 technical publications,

contributing to several IEEE peer-reviewed publications, 3GPP/IEEE standards, as well as holds numerous patents. Prior to Intel, Dr. Himayat was with Lucent Technologies and General Instrument Corp, where she developed standards and systems for both wireless and wire-line broadband access networks. Dr. Himayat obtained her B.S.E.E degree from Rice University, and her Ph.D. degree from the University of Pennsylvania. She also holds an MBA degree from the Haas School of Business at University of California, Berkeley.



Yevgeni Koucheryavy is a Full Professor in the Laboratory of Electronics and Communications Engineering of Tampere University, Finland. He received his Ph.D. degree (2004) from Tampere University of Technology. He is the author of numerous publications in the field of advanced wired and wireless networking and communications. His current research interests include various aspects in heterogeneous wireless communication networks and systems, the Internet of Things

and its standardization, as well as nanocommunications. He is Associate Technical Editor of IEEE Communications Magazine and Editor of IEEE Communications Surveys and Tutorials.

1

Spatially-Consistent Human Body Blockage Modeling: A State Generation Procedure

Margarita Gapeyenko, Andrey Samuylov, Mikhail Gerasimenko, Dmitri Moltchanov, Sarabjot Singh, Mustafa Riza Akdeniz, Ehsan Aryafar, Sergey Andreev, Nageen Himayat, and Yevgeni Koucheryavy

APPENDIX A PROOF OF LEMMA 1

Here, the proof of Lemma 1 is explained in details. First, note that the denominator of

$$p_{10} = \frac{\mathbb{P}\left[\text{M is non-Blocked} \cap \text{O is Blocked}\right]}{\mathbb{P}\left[\text{O is Blocked}\right]}.$$
 (1)

can be written as

earyafar@gmail.com)

$$\mathbb{P}\left[\text{O is Blocked}\right] = \mathbb{P}\left[\left(\widetilde{N}_{2} \cap \widetilde{L}_{4b} \cap \widetilde{L}_{4a}\right) \cup \left(\widetilde{L}_{2} \cap \widetilde{N}_{4b} \cap \widetilde{L}_{4a}\right) \cup \cdots \cup \left(\widetilde{N}_{2} \cap \widetilde{N}_{4b} \cap \widetilde{N}_{4a}\right)\right]. \quad (2)$$

Adding $\widetilde{L}_2 \cap \widetilde{L}_{4b} \cap \widetilde{L}_{4a}$ to the events listed in the right-hand side part of (2), we arrive at the complete event space. Hence, (2) can be simplified to

$$\mathbb{P}\left[\text{O is Blocked}\right] = 1 - \mathbb{P}\left[\widetilde{L}_2 \cap \widetilde{L}_{4b} \cap \widetilde{L}_{4a}\right].$$
 (3)

Observe that the event (M is non-Blocked) is equivalent to $L_3 \cap L_{4b} \cap L_{4a}$. Taking into account the fact that the events L_{4a} and \widetilde{N}_{4a} are mutually exclusive, the numerator of (1) becomes

$$\begin{split} &\mathbb{P}\left[\text{M is non-Blocked}\cap\text{O is Blocked}\right] = \\ &= \mathbb{P}\left[\left(\widetilde{N}_{2}\cap\widetilde{L}_{4b}\cap\widetilde{L}_{4a}\cap L_{4b}\cap L_{4a}\cap L_{3}\right)\cup\right. \\ &\left. \cup \left(\widetilde{L}_{2}\cap\widetilde{N}_{4b}\cap\widetilde{L}_{4a}\cap L_{4b}\cap L_{4a}\cap L_{3}\right)\cup\right. \\ &\left. \cup \left(\widetilde{N}_{2}\cap\widetilde{N}_{4b}\cap\widetilde{L}_{4a}\cap L_{4b}\cap L_{4a}\cap L_{3}\right)\right] = \\ &= \mathbb{P}\left[L_{3}\cap\left(\left(\widetilde{N}_{2}\cap\widetilde{L}_{4b}\cap\widetilde{L}_{4a}\cap L_{4b}\cap L_{4a}\right)\cup\right. \\ &\left. \cup \left(\widetilde{N}_{4b}\cap\widetilde{L}_{4a}\cap L_{4b}\cap L_{4a}\right)\right)\right]. \end{split} \tag{4}$$

The event $\widetilde{N}_{4b} \cap L_{4b}$ corresponds to having at least one blocker occluding the link path at O, while all of them are not high enough to block the link at M.

M. Gapeyenko, A. Samuylov, M. Gerasimenko, D. Moltchanov, S. Andreev, and Y. Koucheryavy are with Tampere University, Tampere, Finland (e-mail: {firstname.lastname, evgeni.kucheryavy}@tuni.fi).
S. Singh is with Ulnana (e-mail: sarabjotsingh.in@gmail.com)
M. R. Akdeniz and N. Himayat are with Intel Corporation, Santa Clara, CA, USA (e-mail: {mustafa.akdeniz, nageen.himayat}@intel.com)
E. Aryafar is with Portland State University, Portland, OR, USA (e-mail:

Hence, accounting for (4), the probability that M is non-blocked given that O is blocked can be obtained as

$$p_{10} = \frac{\mathbb{P}_{nb3} \left(\widetilde{\mathbb{P}}_{b2} \widetilde{\mathbb{P}}_{nb4b} \mathbb{P}_{nb4a} + \mathbb{P}_{nb4b}^* \mathbb{P}_{nb4a} \right)}{1 - \widetilde{\mathbb{P}}_{nb2} \widetilde{\mathbb{P}}_{nb4a} \widetilde{\mathbb{P}}_{nb4b}}, \quad (5)$$

APPENDIX B DERIVATION OF GEOMETRICAL PARAMETERS

Here, we estimate the distances in the scenario that are required by the proposed framework.

Aligning the center of the Cartesian coordinate system at 0 and OY axis with OP, the coordinates of points A, B, C, and D are given by

$$x_A = 0$$
, $x_B = 0$, $x_C = d_m$, $x_D = d_m$,
 $y_A = 0$, $y_B = r_0$, $y_C = r_0$, $y_D = 0$. (6)

The coordinates of E, H, G, and F are thus

$$x_E = \frac{d_m}{2} + d_0 \sin \alpha - \frac{d_m}{2} \cos \beta,$$

$$y_E = d_0 \cos \alpha - \frac{d_m}{2} \sin \beta,$$

$$x_H = x_E + d_m \cos \beta, \quad y_H = y_E + d_m \sin \beta,$$

$$x_G = x_H - r_1 \sin \beta, \quad y_G = y_H + r_1 \cos \beta,$$

$$x_F = x_G - d_m \cos \beta, \quad y_F = y_G - d_m \sin \beta,$$
(7)

where r_1 and β are given by

$$r_1 = \sqrt{r_0^2 + d_0^2 - 2r_0 d_0 \cos \alpha},$$

$$\beta = \arcsin\left(\frac{d_0 \sin \alpha}{r_1}\right).$$
(8)

The coordinates of K, the intersection of CD with FE, are

$$x_K = d_m, \quad y_K = (d_m - x_F) \frac{y_E - y_F}{x_E - x_E} + y_F.$$
 (9)

The length of KE is

$$|KE| = \sqrt{(x_E - x_K)^2 + (y_E - y_K)^2}.$$
 (10)

The coordinates of the intersection between LD and GH, I, are

$$x_I = d_m, \quad y_I = (d_m - x_G) \frac{y_H - y_G}{x_H - x_G} + y_G.$$
 (11)

The lengths of IK and IJ are

$$|IK| = \sqrt{(x_K - x_I)^2 + (y_K - y_I)^2};$$

$$|IJ| = \sqrt{|IK|^2 - d_m^2}.$$
(12)

To determine the probability of having no blockers that affect the LoS path at M in zone 4, two parts of two planes (ABC) and (EFG) will be considered with the following z coordinates: $(z_B = h_C; z_C = h_C; z_D = h_1)$ and (EFG) $(z_F = h_C; z_G = h_C; z_H = h_2)$. The equation for (ABC) is

$$ax - by + cz + (-ax_C + by_C - cz_C) = 0,$$
 (13)

where the coefficients a, b, and c are given by

$$a = (y_B - y_C)(z_D - z_C) - (y_D - y_C)(z_B - z_C),$$

$$b = (x_B - x_C)(z_D - z_C) - (x_D - x_C)(z_B - z_C),$$

$$c = (x_B - x_C)(y_D - y_C) - (x_D - x_C)(y_B - y_C).$$
 (14)

The equation for (EFG) reads as

$$fx - qy + hz + (-fx_G + qy_G - hz_G) = 0,$$
 (15)

where the constants f, g, and h are

$$f = (y_F - y_G)(z_H - z_G) - (y_H - y_G)(z_F - z_G),$$

$$g = (x_F - x_G)(z_H - z_G) - (x_H - x_G)(z_F - z_G),$$

$$h = (x_F - x_G)(y_H - y_G) - (x_H - x_G)(y_F - y_G).$$
 (16)

Further, we require the equation for a segment PU, the intersection of two planes ABC and FGH as follows

$$\frac{x}{gc - bh} = \frac{y - y_Q}{cf - ah} = \frac{z - z_Q}{bf - ag},\tag{17}$$

where y_O and z_O are

$$y_Q = \frac{cz_Q + d}{b}, z_Q = \frac{gd - be}{bh - gc}.$$
 (18)

while d and e are:

$$d = -ax_C + by_C - cz_C, e = -fx_G + gy_G - hz_G.$$
 (19)

We also find the intersection point W of CD and PU with the coordinates

$$x_{W} = d_{m},$$

$$y_{W} = \frac{d_{m}(cf - ah)}{(gc - bh)} + y_{Q},$$

$$z_{W} = \left(\frac{d_{m}(cf - ah)}{-r_{0}(gc - bh)} - \frac{y_{Q}}{r_{0}} + 1\right)$$

$$\left(h_{1} - h_{C}\right) + h_{C}.$$
(20)

The coordinates of T are given by

$$x_{T} = \frac{(x_{W} - x_{P})(y_{P}x_{R} - y_{N}x_{R})}{(y_{R} - y_{N})(x_{W} - x_{P}) - x_{R}(y_{W} - y_{P})}$$

$$\frac{x_{R}x_{P}(y_{W} - y_{P})}{(y_{R} - y_{N})(x_{W} - x_{P}) - x_{R}(y_{W} - y_{P})},$$

$$y_{T} = \frac{x_{T}(y_{R} - y_{N})}{x_{R}} + y_{N},$$
(21)

where the coordinates of P and N are

$$x_P = \frac{d_m}{2}, \quad x_N = 0,$$

 $y_P = r_0, \quad y_N = r_0 - \frac{d_m}{2}.$ (22)

The lengths of TR and WR are

$$|TR| = \sqrt{(x_R - x_T)^2 + (y_R - y_T)^2};$$

$$|WR| = \sqrt{(x_R - x_W)^2 + (y_R - y_W)^2}.$$
 (23)

The intersection point W' between PU and FE is

$$x_{W'} = \frac{(y_F - y_Q)(gc - bh)(x_E - x_F)}{(cf - ah)(x_E - x_F) - (y_E - y_F)(gc - bh)}$$

$$\frac{x_F(y_E - y_F)(gc - bh)}{(cf - ah)(x_E - x_F) - (y_E - y_F)(gc - bh)},$$

$$y_{W'} = \frac{x_{W'}(cf - ah)}{gc - bh} + y_Q.$$
(24)

The coordinates of T' and S are therefore

$$x_{T'} = x_{W'}; y_{T'} = r_0 - \frac{d_m}{2};$$

$$x_S = \frac{(y_S - y_F)(x_E - x_F)}{y_E - y_F} + x_F;$$

$$y_S = r_0 - \frac{d_m}{2}.$$
 (25)

The lengths of SR, W'T', RK, and ST are

$$|SR| = \sqrt{(x_R - x_S)^2 + (y_R - y_S)^2};$$

$$|W'T'| = \sqrt{(x_{T'} - x_{W'})^2 + (y_{T'} - y_{W'})^2};$$

$$|RK| = \sqrt{(x_K - x_R)^2 + (y_K - y_R)^2};$$

$$|ST| = \sqrt{(x_T - x_S)^2 + (y_T - y_S)^2}.$$
(26)

Intersection of EH and CD is I'.

$$x_{I'} = x_D,$$

 $y_{I'} = \frac{(x_D - x_E)(y_H - y_E)}{x_H - x_E} + y_E.$ (27)

Intersection of FE and AD is K'

$$x_{K'} = \frac{(y_D - y_F)(x_E - x_F)}{y_E - y_F} + x_F,$$

$$y_{K'} = y_D.$$
 (28)

Intersection of AD and EH is D'.

$$x_{D'} = \frac{(y_D - y_E)(x_H - x_E)}{y_H - y_E} + x_E,$$

$$y_D = y_D.$$
 (29)

Intersection of PU and AD is U'.

$$x_{U'} = \frac{(y_D - y_Q)(gc - bh)}{cf - ah},$$

$$y_{U'} = y_D.$$
 (30)

Intersection of PU and EH is E'.

$$x_{E'} = \frac{x_E(y_H - y_E)(gc - bh)}{(y_H - y_E)(gc - bh) - (cf - ah)(x_H - x_E)},$$

$$\frac{(y_Q - y_E)(x_H - x_E)(gc - bh)}{(y_H - y_E)(gc - bh) - (cf - ah)(x_H - x_E)},$$

$$y_{E'} = \frac{x_{E'}(cf - ah)}{qc - bh} + y_Q.$$
(31)

All below coordinates belong to the projection of the point required for calculating the area in question. The coordinates of D'', W'', T'', E'', and H' are:

$$\begin{cases} x_{D''} = x_{D'} \\ x_{W''} = x_{W'} \\ x_{T''} = x_{T} \\ x_{E''} = x_{E'} \\ x_{H'} = x_{E} \end{cases}, \begin{cases} y_{D''} = y_{R} \\ y_{W''} = y_{R} \\ y_{T''} = y_{D} \\ y_{E''} = y_{R} \\ y_{H'} = y_{D} \end{cases}$$
(32)

Our technical report [1] collects all the cases with the required limits of integration. The expressions for some parameters used in our technical report are given next.

$$L_{EF} = \frac{(x - x_F)(y_E - y_F)}{x_E - x_F} + y_F;$$

$$L_{HG} = \frac{(x - x_G)(y_H - y_G)}{x_H - x_G} + y_G;$$

$$L_{HE} = \frac{(x - x_E)(y_H - y_E)}{x_H - x_E} + y_E;$$

$$L_{PU} = \frac{cf - ah}{gc - bh} \cdot x + y_Q.$$
(33)

REFERENCES

[1] A. Samuylov *et al.*, "Characterizing spatial correlation of blockage statistics," Tampere University of Technology, Technical report available at: http://winter-group.net/downloads/mmWave_blockage_report.pdf, 2016.